Detecting and Characterizing the Nonadiabaticity of Laser-Induced Quantum Tunneling

Kunlong Liu,[1,2] Siqiang Luo,[1] Min Li,[1,*] Yang Li,[1] Yudi Feng,[1] Baojie Du,[1] Yueming Zhou,[1]
Peixiang Lu,[1,3,†] and Ingo Barth[2,‡]

[1]*Wuhan National Laboratory for Optoelectronics and School of Physics,*
Huazhong University of Science and Technology, Wuhan 430074, China
[2]*Max-Planck-Institut für Mikrostrukturphysik, Weinberg 2, 06120 Halle (Saale), Germany*
[3]*Hubei Key Laboratory of Optical Information and Pattern Recognition,*
Wuhan Institute of Technology, Wuhan 430205, China

The nonadiabaticity of quantum tunneling through an evolving barrier is relevant to resolving laser-driven dynamics of atoms and molecules at an attosecond timescale. Here, we propose and demonstrate a novel scheme to detect the nonadiabatic behavior of tunnel ionization studied in an attoclock configuration, without counting on the laser intensity calibration or the modeling of the Coulomb effect. In our scheme, the degree of nonadiabaticity for tunneling scenarios in elliptically polarized laser fields can be steered continuously simply with the pulse ellipticity, while the critical instantaneous vector potentials remain identical. We observe the characteristic feature of the measured photoelectron momentum distributions, which matches the distinctive prediction of nonadiabatic theories. In particular, our experiments demonstrate that the nonadiabatic initial transverse momentum at the tunnel exit is approximately proportional to the instantaneous effective Keldysh parameters in the tunneling regime, as predicted theoretically by Ohmi, Tolstikhin, and Morishita [Phys. Rev. A **92**, 043402 (2015)]. Our study clarifies a long-standing controversy over the validation of the adiabatic approximation and will substantially advance studies of laser-induced ultrafast dynamics in experiments.

Tunneling is one of the most important mechanisms for ionization of atoms and molecules by strong laser fields, where the bound electron penetrates the barrier formed by the Coulomb field and the electric field [1]. However, instead of being static, the near-infrared laser field oscillates periodically (~2.6 fs per optical cycle, typically), resulting in a time-dependent barrier and thus making the tunneling a rather intricate process [2]. The "nonadiabaticity" of the tunneling process has attracted great attention in the past decades [3–5], as it is of vital importance in interpreting the ultrafast phenomena following tunnel ionization [6].

The degree of nonadiabaticity for strong-field tunneling is usually characterized by the Keldysh parameter $\gamma = (\omega/\mathcal{E})\sqrt{2I_p}$ [1–3], where I_p is the ionization potential, $\mathcal{E}$ the field strength amplitude, and ω the frequency of the electric field. In general, the condition $\gamma \ll 1$ is considered as the adiabatic limit, whereas the typical condition in the laboratory lies in the regime $\gamma \sim 1$ where the nonadiabatic tunnel ionization occurs. The validation of the adiabatic approximation for strong-field tunnel ionization in attoclock experiments [7] have been widely debated. Though the nonadiabatic effects have been predicted by different theoretical models [1–5,8–16], the conclusions so far from various experimental studies [17–22] are seemingly contradictory. In particular, Arissian *et al.* [17] found no evidence

of nonadiabatic effects by measuring the momentum distribution of photoelectrons along the laser propagation direction, and Boge *et al.* [18] claimed that nonadiabatic theories contradict the experimental trends of the tilted angles of the photoelectron momentum distributions (PMDs) in attoclock measurements, while Eckart *et al.* [20] recently showed evidence of nonadiabatic effects using bicircularly polarized laser pulses.

The experimental tests of nonadiabatic effects are mostly based on the mapping relation between the initial photoelectron momentum and the measured final photoelectron momentum. In the nonadiabatic tunneling picture of atoms (see Fig. 1), the measurable final momentum $\mathbf{p}_f$ is a function of three variables: the initial transverse momentum $\mathbf{p}_0$ that depends on the instantaneous angular frequency and strength of the electric field (theoretical prediction in Ref. [5]), the negative of the instantaneous vector potential $\mathbf{p}_A = -\mathbf{A}(t)$ determined by the laser intensity, and the accumulated momentum drift $\mathbf{p}_C$ caused by the Coulomb effect, i.e.,

$$\mathbf{p}_f = f(\mathbf{p}_0, \mathbf{p}_A, \mathbf{p}_C) = \mathbf{p}_0 + \mathbf{p}_A + \mathbf{p}_C. \qquad (1)$$

Generally, the predicted nonadiabatic momentum offset $\mathbf{p}_0$ is rather small. The long-standing obstacle to experimentally investigating $\mathbf{p}_0$ is the accurate determination of $\mathbf{p}_A$
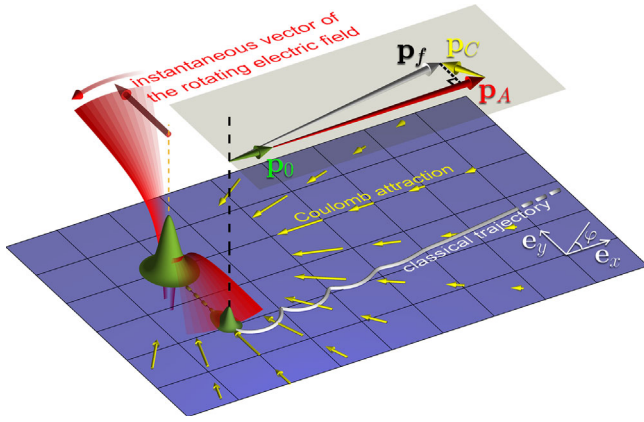
FIG. 1.   The physical picture of the nonadiabatic tunnel ionization of atoms driven by rotating laser fields. See text for details.

and $\mathbf{p}_C$. In previous experimental studies [17–20], calibrating the pulse intensity (for $\mathbf{p}_A$) [17,18] or calculating the Coulomb effect (for $\mathbf{p}_C$) [19,20] relies on the theoretical models that themselves need independent experimental demonstrations in the first place. Thus, controversial even conflicting conclusions would be made if $\mathbf{p}_A$ and $\mathbf{p}_C$ are obtained from various theoretical models. Moreover, it is still challenging to identify the boundary when the adiabatic approximation holds or breaks down.

Key to overcoming the difficulty of determining $\mathbf{p}_A$ and $\mathbf{p}_C$ is a feasible way to continuously steer the degree of nonadiabaticity at the concerned tunneling events while (i) the corresponding instantaneous vector potentials remain identical and (ii) the Coulomb effect is mechanically distinguished from the nonadiabatic effect. Then, we will be able to single out the relation between $\mathbf{p}_f$ and $\mathbf{p}_0$ independently from the measurements. In this Letter, we design a scheme to achieve this goal and characterize the nonadiabaticity of the tunnel ionization in elliptically polarized (EP) fields via the observable PMDs.

The idea is illustrated in Fig. 2. The right EP field is given by $\mathbf{E}(t) = \mathcal{E}_x \cos(\omega t)\mathbf{e}_x + \mathcal{E}_y \sin(\omega t)\mathbf{e}_y$. In our scheme, the field amplitude along the x direction is fixed ($\mathcal{E}_x \equiv \mathcal{E}$), whereas $\mathcal{E}_y$ is variable. Throughout the present study, the
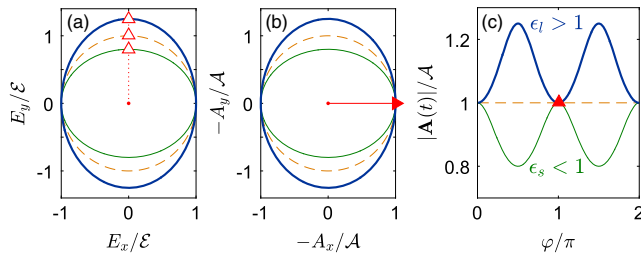

FIG. 2.   The electric fields and vector potentials for $\epsilon_l > 1$ (thick), $\epsilon = 1$ (dashed), and $\epsilon_s < 1$ (thin). The hollow triangles in (a) indicate three scenarios where ionization takes place. Their corresponding vector potentials are identical, as shown by solid triangles in (b) and (c).

ellipticity ϵ is defined as $\epsilon = \mathcal{E}_y/\mathcal{E}_x$, and it could be smaller or larger than 1. The corresponding negative vector potential is given by $-\mathbf{A}(t) = \mathcal{A} \sin(\omega t)\mathbf{e}_x - \epsilon\mathcal{A}\cos(\omega t)\mathbf{e}_y$ with $\mathcal{A} = \mathcal{E}/\omega$. In particular, as shown in Fig. 2(a), at $t = t_0 = (\pi/2)(1/\omega)$, where $\mathbf{E}(t_0) = \epsilon\mathcal{E}\mathbf{e}_y$, the instantaneous field strength and the instantaneous angular frequency are $\mathcal{E}_i = \epsilon\mathcal{E}$ and $\omega_i = \omega/\epsilon$, respectively [23]. Accordingly, we define the instantaneous effective Keldysh parameter at $t = t_0$ as $\gamma_i = (\omega_i/\mathcal{E}_i)\sqrt{2I_p} = [\omega/(\epsilon^2\mathcal{E})]\sqrt{2I_p} = (1/\epsilon^2)\gamma$,   which can be changed continuously via adjusting the ellipticity ϵ. Meanwhile, the corresponding negative vector potential given by $-\mathbf{A}(t_0) = \mathcal{A}\mathbf{e}_x$ remains identical for arbitrary ϵ, as indicated in Figs. 2(b) and 2(c). Note that the critical vector potential marked by the solid triangle is maximal if $\epsilon < 1$ and minimal if $\epsilon > 1$.

Next, let us look into the tunneling scenarios at $t = t_0$. For simplicity, two cases for different ellipticities ($\epsilon_s < 1 < \epsilon_l$) are discussed. In the adiabatic frame without considering the Coulomb effect, the maximal final photoelectron momentum drift for ϵ_s and the minimal one for ϵ_l would satisfy $|\mathbf{p}_{f,s}|_{\max} = |\mathbf{p}_{f,l}|_{\min}$ because of the identical vector potentials [see Fig. 2(c)]. In the further situation where the Coulomb effect is included, the centripetal Coulomb attraction decelerates the photoelectron [24]. Given that the overall field strength for ϵ_s is not greater than that for the relatively larger ellipticity ϵ_l [see Fig. 2(a)], the Coulomb effect is more significant for ϵ_s, as the photoelectron is less energetic and spends more time interacting with the ion. Thus, under the adiabatic assumption, the phenomenon $|\mathbf{p}_{f,s}|_{\max} < |\mathbf{p}_{f,l}|_{\min}$ is expected. On the other hand, however, the nonadiabatic effect would cause a nonzero initial momentum of the photoelectron. According to the first-order nonadiabatic correction in the adiabatic theory [5], the final momentum drift for $t = t_0$ can be expressed as (neglecting the Coulomb effect) [25]

$$|\mathbf{p}_f| = p_x = \mathcal{A} + \frac{\sqrt{2I_p}}{6}\gamma_i, \qquad (2)$$

where the term $(\sqrt{2I_p}/6)\gamma_i$ is the initial transverse momentum arising from the nonadiabaticity of tunneling. Since $\gamma_i = (1/\epsilon^2)\gamma$, the larger ϵ, the smaller γ_i, and, consequently, the smaller is the initial transverse momentum at the tunnel exit and vice versa. Because of the fixed $\mathcal{A}$ in our scheme, $|\mathbf{p}_{f,s}|_{\max} > |\mathbf{p}_{f,l}|_{\min}$ should be observed according to the nonadiabatic tunneling picture. Therefore, within our scheme, the nonadiabatic effect acts against the Coulomb effect on the final photoelectron momentum drift. The characteristic feature of the observable momentum drifts for different ellipticities will be a direct test of the nonadiabatic effect, without counting on the calibration of the laser intensity or the theoretical modeling of the Coulomb effect.

Based on the scheme described above, we measured the PMDs for Ne atoms using a cold target recoil ion momentum spectroscopy (COLTRIMS). The laser pulses
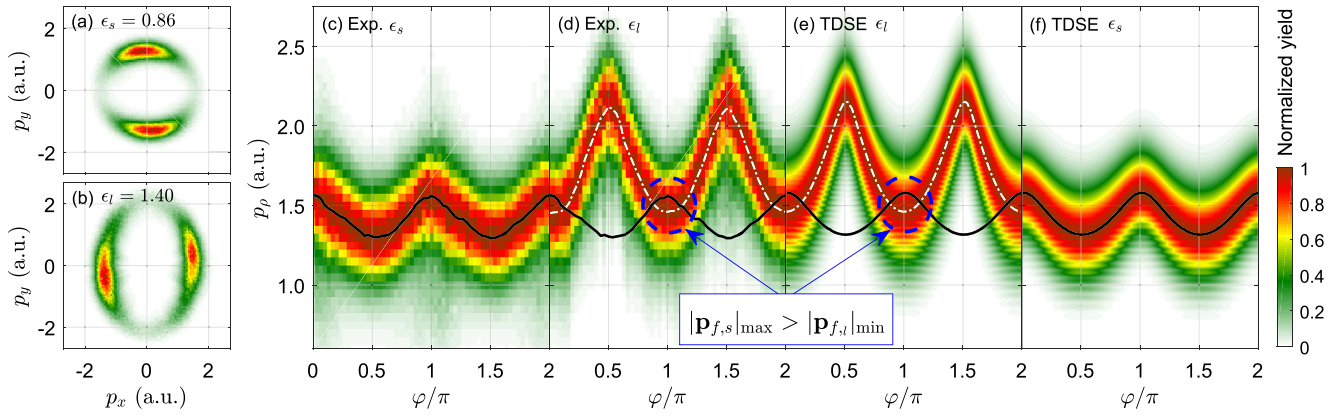
FIG. 3. The PMDs [(a) and (b)] and normalized momentum-resolved PADs [(c)–(f)] for $\epsilon_s = 0.86$ and $\epsilon_l = 1.40$ obtained from experiments and TDSE simulations. The photoelectron momentum drift as a function of the emission angle for ϵ_s and ϵ_l is shown by solid and dash-dotted curves, respectively. The distinct momentum drifts at $\varphi \approx \pi$ (and $\varphi \approx 0$) for two ellipticities are evidence for the nonadiabatic tunnel ionization.

were generated by an amplified Ti:sapphire femtosecond laser system with a repetition rate of 5 kHz centered at 800 nm. The pulse duration was approximately 40 fs. We used a wire grid polarizer before a $\lambda/4$ wave plate to control the polarization ellipse of the laser pulse. The fast axis of the $\lambda/4$ wave plate was fixed along the x direction. Before each acquisition of experimental data, we adjusted the total input pulse intensity and used a second wire grid polarizer to check and ensure that the component of the pulse intensity along the x axis was constant for varying ellipticities. The laser pulse was then focused into the supersonic beam in the main chamber of the COLTRIMS system by a parabolic mirror ($f = 75$ mm). A uniformed electric field about 41 V/cm and a uniformed magnetic field about 19 G were used to collect the photoelectrons and photoions. The three-dimensional momenta of the electrons and ions were reconstructed from the time of flights and the positions of the particles on the detectors.

The measured PMDs for $\epsilon_s = 0.86$ and $\epsilon_l = 1.40$ are shown in Figs. 3(a) and 3(b), respectively, corresponding to the total pulse intensities of approximately 0.38 and 0.65 PW/cm^2. The tilted angles of the two-lobe structures with respect to the laser ellipse are mainly contributed by the Coulomb attraction [7,12] and, possibly, the non-adiabatic effect [5]. To obtain the momentum drift as a function of the emission angle φ, we show the corresponding momentum-resolved photoelectron angular distributions (PADs) in Figs. 3(c) and 3(d). The PADs are normalized to the maximal yields at each angle since we are interested in the momentum drift instead of the instantaneous ionization rate. For comparison, we have also performed numerical simulations based on the time-dependent Schrödinger equation (TDSE) for Ne [26]. The simulated results [27] for $\mathcal{E} = 0.079$ a.u. and the same ellipticities as in experiments are shown in Figs. 3(e) and 3(f). The simulated PADs exhibit very good agreement with those observed in experiments. As indicated by the dashed

circles in Figs. 3(d) and 3(e), the crossings between the two curves mean that the maximal momentum drift for ϵ_s is larger than the minimal one for ϵ_l, i.e., $|\mathbf{p}_{f,s}|_{\max} > |\mathbf{p}_{f,l}|_{\min}$. Following the scheme described above via Fig. 2, it demonstrates that two distinct nonzero initial momenta are caused by the nonadiabatic effect and that the adiabatic approximation breaks down. Note that the conclusion here does not rely on the specification of the intensity used in the simulations. Here, the observed crossing structure can be intuitively explained within the adiabatic theory [4,5]. According to Eq. (2), since $\gamma_{i,s}/\gamma_{i,l} = \epsilon_l^2/\epsilon_s^2 > 1$, a larger nonadiabatic initial transverse momentum for ϵ_s would be added to the fixed critical vector potential (see Fig. 2). Eventually, it leads to a larger final momentum drift for ϵ_s than that for ϵ_l at $\varphi \approx 0$ and $\varphi \approx \pi$.

For further understanding of the underlying mechanism when the Coulomb effect is included, we perform the classical trajectory Monte Carlo (CTMC) simulations [19] using the same laser parameters as in the TDSE simulations. In the CTMC models, the initial coordinates of the tunneled electron are given by either the ADK theory [28] (adiabatic approximation) or the nonadiabatic theory based on the strong-field approximation (SFA) [29,30]. Starting with the initial coordinates, i.e., the tunnel exit and the initial momentum distributions, we calculate the PMDs by numerically solving the classical Newtonian equation with consideration of the Coulomb potential [19]. Figure 4 presents the momentum drifts obtained from the experimental data and from the results based on the nonadiabatic CTMC model with the Coulomb effect, as well as on the adiabatic CTMC models without or with the Coulomb effect.

Figures 4(a)–4(c) show that, within our experimental scheme, the predictions of various theoretical models differ from each other. In particular, the models based on the nonadiabatic theory and the adiabatic approximation (without or with the Coulomb effect) show distinctive observable features of the momentum drifts, i.e., crossing, cutting, and
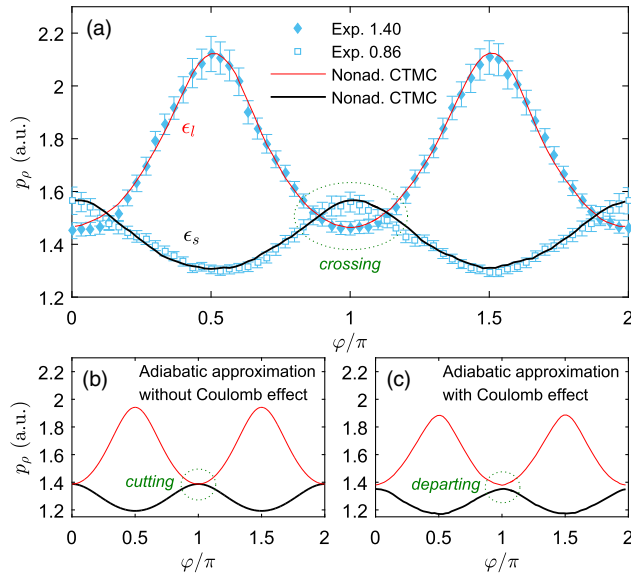
FIG. 4.   The angular dependence of the photoelectron momentum drift obtained from (a) experimental measurements (markers) and simulations based on the nonadiabatic CTMC model (solid lines) with the Coulomb effect, as well as on the adiabatic CTMC models (b) without and (c) with the Coulomb effect. In these three models, the curves for ϵ_s and ϵ_l exhibit distinctive relations: crossing, cutting, and departing, respectively.

FIG. 5.   The dependence of the final photoelectron momentum drift on the ellipticity and the instantaneous effective Keldysh parameter γ_i based on different methods. See text for details.

departing, respectively. Therefore, by measuring the PMDs and comparing the observed feature with the predictions, one can determine which model is more accurate. Since the measurements shown in Fig. 4(a) match the crossing structure, we can conclude that the nonadiabatic effect certainly plays an indispensable role in laser-induced tunneling dynamics. Moreover, one can find that the crossing structures of the experimental observations and the non-adiabatic CTMC simulations agree with the prediction of Eq. (2) from the adiabatic theory [5].

Last but not least, we inspect the validation of adiabatic approximation over a range of the instantaneous effective Keldysh parameters γ_i via changing the ellipticity within our scheme. In Fig. 5, we depict the final momentum drift as a function of the ellipticity and the corresponding instantaneous effective Keldysh parameter γ_i. The results are extracted from the PADs at $\varphi = \pi$ based on experiments, TDSE simulations, and the nonadiabatic and adiabatic CTMC simulations with the Coulomb effect. The momentum drifts given by the adiabatic theory [5], as well as those within the adiabatic approximation, are also shown in Fig. 5. The field strength amplitude $\mathcal{E} = 0.079$ a.u. is applied for all theoretical methods. The range of ellipticity from 1.51 to 0.64 corresponds to the instantaneous effective Keldysh parameter ranging from 0.4 to 2.2 and to the instantaneous field strength from 0.12 to 0.05 a.u.

One can see from Fig. 5 that, within the adiabatic CTMC simulations, the critical final momentum drift decreases
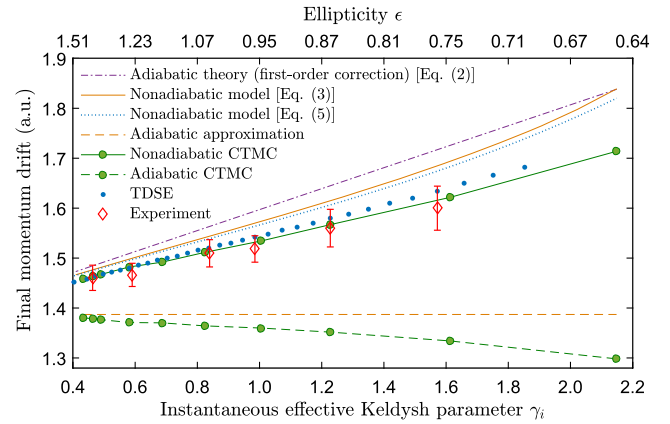
with the increasing γ_i due to the enhancing Coulomb effect. In contrast, the momentum drifts observed in experiments exhibit the tendency to increase with increasing γ_i, and the theoretical models which include the nonadiabatic effect reproduce the coinciding phenomenon. Given that the critical vector potential is identical for arbitrary ellipticity, the observation shown in Fig. 5 proves that the initial transverse momentum induced by the nonadiabatic effect is approximately proportional to γ_i in the regime of $\gamma_i \sim 1$.

For comparison, we further derive an analytic expression for the momentum drift based on the SFA [29,30] for the present scheme. The transition rate from the ground state to the continuum state **p** can be calculated within exponential accuracy $W \propto \exp(-2\,\mathrm{Im}\,S)$, where $S = \frac{1}{2}\int_0^{t_i}[\mathbf{p} + \mathbf{A}(t')]^2 dt' + I_p t_i$ is the action under the barrier, $t_i = t_0 + i\tau$ is the complex ionization time (also referred to as the solution of the saddle-point equation) that can be interpreted as the time of entering into the barrier, $t_0 = \mathrm{Re}\,t_i$ is the time of exiting the barrier, and $\tau = \mathrm{Im}\,t_i$ is the tunneling time [31,32]. By deriving the imaginary part of the action, one can eventually obtain the most probable final drift momentum

$$p_x = \frac{\mathcal{E}}{\omega}\frac{\sinh(\omega\tau)}{\omega\tau}, \qquad (3)$$

where the tunneling time τ satisfies the transcendental equation

$$\sinh^2(\omega\tau)\left[\epsilon^2 - \left(\coth(\omega\tau) - \frac{1}{\omega\tau}\right)^2\right] = \gamma^2. \qquad (4)$$

The associated initial transverse momentum can be calculated by $v_x = p_x - \mathcal{A}$. The nonadiabatic model introduced above is valid for the tunneling occurring along the major and minor axes of the laser ellipse. By expanding the momentum drift in Eq. (3) in Taylor series with respect to the instantaneous effective Keldysh parameter, we obtain the analytical expression for the momentum drift (up to the third order) [25]

$$p_x = \frac{\mathcal{E}}{\omega} + \frac{\sqrt{2I_p}}{6}\gamma_i + \frac{\sqrt{2I_p}}{6}\left(\frac{1}{9} - \frac{17}{60}\epsilon^2\right)\gamma_i^3. \quad (5)$$

One can find that the first-order term in Eq. (5) is the same as that in Eq. (2). The results obtained from Eqs. (3) and (5) (solid and dotted curves, respectively) depicted in Fig. 5 agree with the trend of the measurements. It clearly demonstrates the nonadiabatic behavior of tunnel ionization in rotating fields.

Moreover, we find in Fig. 5 that the nonadiabatic momentum offset is still not negligible even for the Keldysh parameters as low as 0.4, where the instantaneous field strength and the angular frequency correspond to a 1200-nm circularly polarized laser pulse with the pulse intensity of 10^{15} W/cm^2. It suggests that, in general, the adiabatic approximation for tunnel ionization in a rotating field is inaccurate under the typical conditions in the laboratory.

In conclusion, we have demonstrated an experimental scheme which reveals the nonadiabaticity of strong-field tunnel ionization, without counting on the laser intensity calibration. The scheme also mechanically distinguishes the nonadiabatic effect from the Coulomb effect on photoelectrons. As the characteristic feature of the nonadiabatic effect on the tunneling electron, the observed crossing structure in Fig. 4(a) demonstrates straightforwardly and unambiguously the association of the initial transverse momentum of the tunneling electronic wave packet with the instantaneous effective Keldysh parameter in EP laser fields. The present study will help refine experimental observations in the future and has significant implications in the appealing strong-field phenomena which are triggered by tunnel ionization in rotating laser fields, e.g., elliptically polarized high-harmonic generation [33], nonsequential double ionization [34], spin polarization [35], and photoelectron holography [36].

*mli@hust.edu.cn
†lupeixiang@hust.edu.cn
‡barth@mpi-halle.mpg.de

[1] M. Y. Ivanov, M. Spanner, and O. Smirnova, J. Mod. Opt. **52**, 165 (2005).
[2] A. M. Perelomov, V. S. Popov, and M. V. Terent'ev, Sov. Phys. JETP **23**, 924 (1966); **24**, 207 (1967); A. M. Perelomov and V. S. Popov, Sov. Phys. JETP **25**, 336 (1967).
[3] S. V. Popruzhenko, J. Phys. B **47**, 204001 (2014).
[4] O. I. Tolstikhin and T. Morishita, Phys. Rev. A **86**, 043417 (2012).
[5] M. Ohmi, O. I. Tolstikhin, and T. Morishita, Phys. Rev. A **92**, 043402 (2015).
[6] F. Krausz and M. Ivanov, Rev. Mod. Phys. **81**, 163 (2009).
[7] P. Eckle, A. N. Pfeiffer, C. Cirelli, A. Staudte, R. Dörner, H. G. Muller, M. Büttiker, and U. Keller, Science **322**, 1525 (2008).
[8] D. I. Bondar, Phys. Rev. A **78**, 015405 (2008).
[9] K. Liu and I. Barth, Phys. Rev. A **94**, 043402 (2016).
[10] J. Henkel, M. Lein, V. Engel, and I. Dreissigacker, Phys. Rev. A **85**, 021402(R) (2012).
[11] J.-W. Geng, W.-H. Xiong, X.-R. Xiao, L.-Y. Peng, and Q. Gong, Phys. Rev. Lett. **115**, 193001 (2015).
[12] L. Torlina, F. Morales, J. Kaushal, I. Ivanov, A. Kheifets, A. Zielinski, A. Scrinzi, H. G. Muller, S. Sukiasyan, M. Ivanov, and O. Smirnova, Nat. Phys. **11**, 503 (2015).
[13] C. Hofmann, T. Zimmermann, A. Zielinski, and A. S. Landsman, New J. Phys. **18**, 043011 (2016).
[14] H. Ni, U. Saalmann, and J.-M. Rost, Phys. Rev. Lett. **117**, 023002 (2016).
[15] M. Klaiber, K. Z. Hatsagortsyan, and C. H. Keitel, Phys. Rev. Lett. **114**, 083001 (2015).
[16] K. Liu, H. Ni, K. Renziehausen, J.-M. Rost, and I. Barth, Phys. Rev. Lett. **121**, 203201 (2018).
[17] L. Arissian, C. Smeenk, F. Turner, C. Trallero, A. V. Sokolov, D. M. Villeneuve, A. Staudte, and P. B. Corkum, Phys. Rev. Lett. **105**, 133002 (2010).
[18] R. Boge, C. Cirelli, A. S. Landsman, S. Heuser, A. Ludwig, J. Maurer, M. Weger, L. Gallmann, and U. Keller, Phys. Rev. Lett. **111**, 103003 (2013).
[19] M. Li, M.-M. Liu, J.-W. Geng, M. Han, X. Sun, Y. Shao, Y. Deng, C. Wu, L. Y. Peng, Q. Gong, and Y. Liu, Phys. Rev. A **95**, 053425 (2017).
[20] S. Eckart, K. Fehre, N. Eicke, A. Hartung, J. Rist, D. Trabert, N. Strenger, A. Pier, L. Ph. H. Schmidt, T. Jahnke, M. S. Schöffler, M. Lein, M. Kunitski, and R. Dörner, Phys. Rev. Lett. **121**, 163202 (2018).
[21] D. Shafir, H. Soifer, B. D. Bruner, M. Dagan, Y. Mairesse, S. Patchkovskii, M. Y. Ivanov, O. Smirnova, and N. Dudovich, Nature (London) **485**, 343 (2012).
[22] N. Camus, E. Yakaboylu, L. Fechner, M. Klaiber, M. Laux, Y. Mi, K. Z. Hatsagortsyan, T. Pfeifer, C. H. Keitel, and R. Moshammer, Phys. Rev. Lett. **119**, 023201 (2017).
[23] The instantaneous angular velocity ω_i for the elliptically polarized laser field is calculated as $\omega_i = \partial\varphi_i/\partial t = \epsilon\omega(\mathcal{E}/\mathcal{E}_i)^2$, where φ_i is the direction of $\mathbf{E}(t)$ and $\mathcal{E}_i = |\mathbf{E}(t)|$ is the instantaneous field amplitude. Therefore, for $t = t_0 = (\pi/2)(1/\omega)$, we have $\mathcal{E}_i = \epsilon\mathcal{E}$ and, thus, $\omega_i = \omega/\epsilon$.
[24] K. Liu and I. Barth, Phys. Rev. Lett. **119**, 243204 (2017).
[25] See Supplemental Material at http://link.aps.org/supplemental/10.1103/PhysRevLett.122.053202 for the details of the adiabatic theory and the nonadiabatic model for the photoelectron momentum in elliptically polarized laser fields.

[26] I. Barth and M. Lein, J. Phys. B **47**, 204016 (2014).

[27] The electric field for numerical simulations is defined as $\mathbf{E}(t) = f(t)\mathcal{E}[\cos(\omega t + \phi_{CE})\mathbf{e}_x + \epsilon \sin(\omega t + \phi_{CE})\mathbf{e}_y]$ with $f(t) = \sin^2(\omega t/8)$, where ϕ_{CE} is the carrier-envelope phase ranging from 0 to 2π with the step of $\pi/16$ in our calculations. All numerical results have been averaged over ϕ_{CE} and initial states for $2p_+$ and $2p_-$ orbitals.

[28] M. V. Ammosov, N. B. Delone, and V. P. Krainov, Sov. Phys. JETP **64**, 1191 (1986).

[29] P. Salieres et al., Science **292**, 902 (2001).

[30] W. Becker, F. Grasbon, D. Kopold, D. B. Milošević, G. G. Paulus, and H. Walther, Adv. At. Mol. Opt. Phys. **48**, 35 (2002).

[31] I. Barth and O. Smirnova, Phys. Rev. A **87**, 013433 (2013).

[32] J. Tan, Y. Zhou, M. He, Y. Chen, Q. Ke, J. Liang, X. Zhu, M. Li, and P. Lu, Phys. Rev. Lett. **121**, 253203 (2018).

[33] A. Fleischer, O. Kfir, T. Diskin, P. Sidorenko, and O. Cohen, Nat. Photonics **8**, 543 (2014).

[34] H. Kang, K. Henrichs, M. Kunitski, Y. Wang, X. Hao, K. Fehre, A. Czasch, S. Eckart, L. P. H. Schmidt, M. Schöffler, T. Jahnke, X. Liu, and R. Dörner, Phys. Rev. Lett. **120**, 223204 (2018).

[35] K. Liu, K. Renziehausen, and I. Barth, Phys. Rev. A **95**, 063410 (2017).

[36] Y. Li, Y. Zhou, M. He, M. Li, and P. Lu, Opt. Express **24**, 23697 (2016).